Chapter 12

(Sub)-Picosecond Spectral Evolution of Fluorescence Studied with a Synchroscan Streak-Camera System and Target Analysis

Ivo H. M. van Stokkum[1]*, Bart van Oort[2], Frank van Mourik[3], Bas Gobets[4] and Herbert van Amerongen[2]

[1]Department of Physics and Astronomy, Faculty of Sciences, Vrije Universiteit, De Boelelaan 1081, 1081 HV Amsterdam, The Netherlands; [2]Laboratory of Biophysics, Wageningen University, PO Box 8128, 6700 ET Wageningen, The Netherlands; [3]École Polytechnique Fédérale de Lausanne, Laboratory of Ultrafast Spectroscopy, Institut de Sciences et Ingéniérie Chimiques, Lausanne-Dorigny, Switzerland; [4]Image Science Institute, University Medical Center Utrecht, Utrecht, The Netherlands

Summary

A synchroscan streak camera in combination with a spectrograph can simultaneously record temporal dynamics and wavelength of fluorescence representable as an image with time and wavelength along the axes. The instrument response width is about 1% of the time range (of typically 200 ps to 2 ns). The spectral window of 250 nm may lie between 250 and 850 nm. Such spectrotemporal measurements using low excitation intensities

*Author for correspondence, email: ivo@nat.vu.nl

Thijs J. Aartsma and Jörg Matysik (eds): Biophysical Techniques in Photosynthesis II, pp. 000–000.

have become routine. Sophisticated data analysis methods are mandatory to extract meaningful physicochemical parameters from the wealth of information contained in the streak image. In target analysis a kinetic scheme is used in combination with assumptions on the spectra of the species to describe the system. In this chapter the principals of operation of a streak-camera setup are described, along with the fundamental and technical limitations that one encounters. The correction and calibration steps that are needed as well as data processing and analysis are discussed. Several case studies of bioluminescence are presented, with a particularly in-depth analysis of trimeric Photosystem I core particles of the cyanobacterium *Spirulina platensis*.

I. Introduction

Time-resolved fluorescence spectroscopy has proven to be extremely useful in photosynthesis research in the past decades (Sauer and Debreczeny, 1996). Time-correlated single photon timing (TCSPT) has often been the method of choice, since it is relatively cheap, provides excellent signal-to-noise ratios and is rather standardized. It is particularly useful for determining the overall charge-separation time of a variety of photosynthetic systems, and can even be applied to entire cells and chloroplasts. Like all methods, TCSPT has its limitations: the instrument response time is several tens of picoseconds, which is a serious draw-back, for instance when studying individual pigment-protein complexes where relevant processes occur on sub-ps and ps time scales. Extremely careful measurements and deconvolution of the time traces are needed to resolve a time constant of at best ~5 ps. A second limitation of TCSPT is that, commonly, one selects one detection wavelength at a time, and recording the spectral evolution of the fluorescence requires subsequent measurements at different wavelengths. This restriction determines to a large extent the minimum time for data recording.
The temporal instrument response of a synchroscan streak-camera system has a FWHM of a few picoseconds. With deconvolution it is even possible to measure at sub-ps time resolution, which is approaching the resolution of fluorescence up-conversion (Jimenez and Fleming, 1996). Although the streak camera is generally used to record time-resolved fluorescence, it has also been applied to measure time-resolved absorption spectra in the range from ps to ns (Ito et al., 1991). In this chapter, we discuss fluorescence detection with a streak camera in combination with a spectrograph. This allows for simultaneous registration of both the time of emission of a fluorescence photon and the emission wavelength, reducing the measuring time substantially. The fluorescence photons eventually lead to a two-dimensional image on a CCD camera, of which the vertical position indicates the emission time, whereas the horizontal position corresponds to the emission wavelength. An example of such an image (Gobets et al., 2001b) is given in Fig. 1, in which the grey levels reflect the fluorescence intensity as a function of time and wavelength. Such an image contains a wealth of information and it will be discussed in detail how this information can be extracted. Throughout this chapter we will refer to these data as 'the PS I trimer data'.

Two decades ago Campillo and Shapiro (1983) wrote an excellent review on the history and possibilities of the streak camera, including its application to photosynthesis. Measurements were performed without wavelength dispersion and only in a few cases several wavelengths were probed. In the same year Freiberg and Saari (1983) published a detailed article on the possibilities and limitations of obtaining simultaneously time and wavelength information. Ohtani et al. (1990) performed one of the first fluorescence experiments in photobiology in which excellent time resolution (3 ps) was combined with measuring complete spectra, studying bacteriorhodopsin from purple membranes of *Halobacterium halobium*. There are several later reports on similar preparations (Ohtani et al., 1994, 1999; Kamiya et al., 1997; Haacke et al., 2001; van Stokkum et al., 2006). Such single-chromophore systems are generally easier to study than chlorophyll-containing photosynthetic complexes: in photosynthetic systems excitation-energy transfer between chromophores takes place, which in case of too high excitation energies can result in singlet-singlet annihilation, a process that can distort the fluorescence kinetics (Sauer and Debreczeny, 1996).

Abbreviations: Chl – chlorophyll; DAS – decay associated spectrum; EAS – evolution associated spectrum; EET – excitation energy transfer; FWHM – full width at half maximum; IRF – instrument response function; LHC – light harvesting complex; MA – magic angle; PCP – peridinin-chlorophyll protein; PS – Photosystem; SAS – species associated spectrum; SVD – singular value decomposition; TCSPT – time-correlated single photon timing

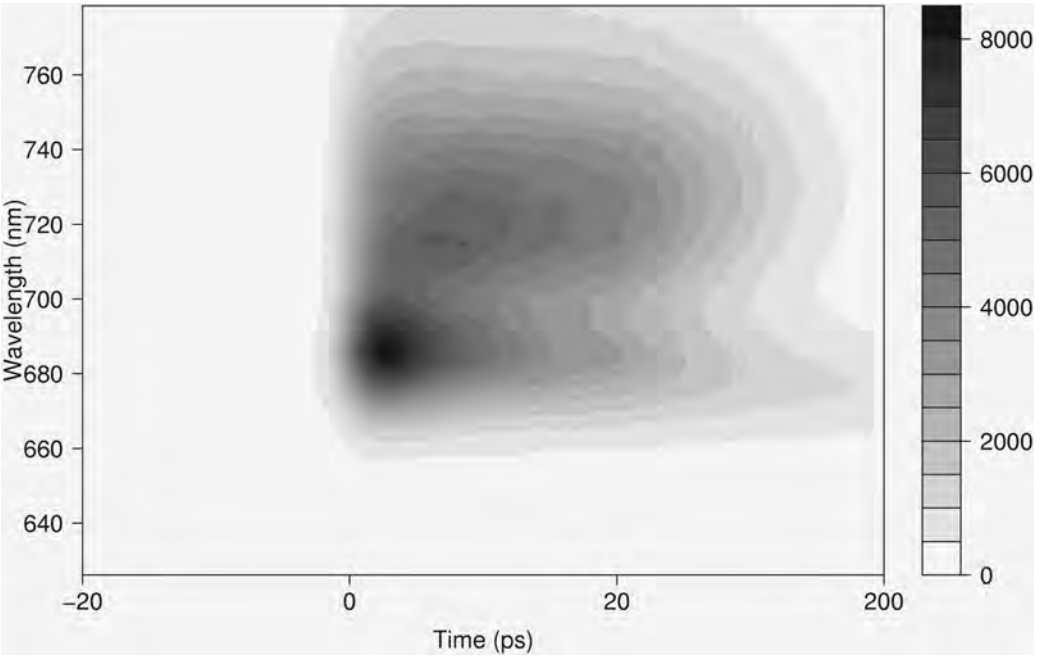

Fig. 1. Filled contour plot of emission data from trimeric core particles of PS I of *Spirulina platensis* (from Gobets et al., 2001b) after excitation at 400 nm. Note that the time axis is linear from –20 to +20 ps relative to the maximum of the IRF, and logarithmic thereafter.

Gilmore et al. (2000, 2003a,b) nicely demonstrated the application of the streak camera to obtain time-resolved fluorescence spectra of leaves. Spectral and kinetic differences between Photosystems I and II could be discerned but relevant spectral evolution was only observed for times longer than 100 ps. Donovan et al. (1997) used a streak camera with 4–9 ps time resolution to study isolated PS II reaction centers. Measuring at multiple wavelengths they concluded that the charge separation time should be either faster than 1.25 ps or slower than 20 ps. Later studies by van Mourik et al. (2004) and Andrizhiyevskaya et al. (2004b) on isolated PS II reaction centers revealed at least four different lifetimes. For excitation at 681 nm lifetimes of 6 ps, 34 ps, 160 ps and 7 ns were observed. The corresponding decay-associated spectra (DAS) were all different except for the 160 ps and 7 ns DAS, indicating that relatively slow excitation energy transfer (EET) takes place. The 34 ps component was assigned to partly represent EET. Further evidence for slow EET was obtained by the fact that excitation at 690 nm resulted in different DAS. In addition, the data indicated that charge separation is ultrafast (<1 ps) and that relatively slow radical pair relaxation takes place.

The streak camera has been particularly useful for the study of fast kinetics in PS I (Gobets et al., 2001a,b; Kennis et al., 2001; Ihalainen et al., 2002, 2005c,d; Andrizhiyevskaya et al., 2004a). Much spectral evolution occurs on a time scale of several ps and higher, which makes PS I an ideal candidate for streak-camera measurements. Below we will make use of some of these results to demonstrate the experimental possibilities of the setup and the power of advanced data analysis.

The streak camera was also used for the study of light-harvesting complexes. It was for instance used to measure lifetimes on the order of many hundreds of ps to several ns and fluorescence quantum yields (Monshouwer et al., 1997; Palacios et al., 2002; Ihalainen et al., 2005a,b). Gobets et al. (2001a) studied LHC-I by fluorescence up-conversion at five different wavelengths (IRF 150 fs, time range 5 ps) and with the streak camera (IRF 3 ps/20 ps , time range 200 ps/2.2 ns) and at common wavelengths the kinetic traces of both techniques joined smoothly in the overlapping time interval. A multitude of decay times was observed ranging from 150 fs to 2 ns (four orders of magnitude) and the corresponding spectra revealed many pathways of EET between carotenoids, Chls *b*, Chls *a* and 'red' Chls *a*, the fluorescence of which is shifted to the red by tens of nm as com-

pared to 'normal' Chls *a*. Analogously, Kennis et al. (2001) demonstrated the applicability of combining fluorescence up-conversion and streak data on PS I core complexes.

One more streak-camera study on a light-harvesting complex is worth mentioning. Kleima et al. (2000) measured the polarized fluorescence of the peridinin-chlorophyll protein (PCP) and EET between isoenergetic Chl *a* molecules over various distances was reflected by different depolarization times. These results will be discussed in more detail below.

In this chapter, we will first describe the principals of operation of a streak-camera setup, followed by a more detailed description of the experimental setup in Wageningen and a discussion of the fundamental and technical limitations that one encounters. In particular, special precautions have to be taken to prevent sample degradation and one has to be aware of the possible occurrence of unwanted nonlinear effects such as singlet-singlet annihilation. In order to exploit the full potential of the setup and the recorded data, several correction and calibration steps are needed as well as advanced data processing and fitting, which will be discussed subsequently.

II. Principle of Operation of the Streak-Camera Setup

The basic goal of the streak-camera setup (Fig. 2) is to determine the wavelength and time of emission of each fluorescence photon detected. A pulsed light source induces fluorescence photons from the sample, which are diffracted by a grating in a horizontal plane after which they hit a horizontal photocathode, producing photo-electrons. These photo-electrons from the photocathode are accelerated and imaged by electrostatic or magnetic lenses onto a 2D detector consisting of a micro-channel plate (MCP) electron multiplier, a phosphor screen, and a cooled CCD camera. On their way from the cathode to the MCP the electrons produced at different times experience a time-dependent vertical electric field (the deflection field or sweep field). Thus photo-electrons generated at different times experience a changed electric field, and therefore hit the MCP at different vertical positions. In the MCP each accelerated photo-electron causes a cascade of electrons (electron multiplication) which in turn hit the phosphor screen, causing a number of photons then detected by the CCD camera. Thus, the vertical and horizontal axes of the 2D CCD-image code respectively for time and wavelength. The time-dependence of the magnitude of the deflection field is sinusoidal and its frequency is locked to the frequency of the same optical oscillator that produces the exciting laser pulses (synchroscan). Thus the streak image on the CCD camera can be accumulated over many successive laser pulses, whilst maintaining a good temporal resolution.

A. Excitation

In the setup in Wageningen, which is comparable to the one in Amsterdam, a mode-locked titanium-sapphire laser, pumped by a 5-W CW diode pumped frequency doubled Nd:YVO_4 laser, provides light pulses at a repetition rate of 75.9 MHz, wavelength 800 nm, 1 W average power and 0.2 ps pulse width. The laser beam is split into two paths: Path 1 is used for synchronization of the deflection field. Path 2 enters a regenerative amplifier (RegA), pumped by a 10 W CW diode-pumped frequency-doubled Nd:YVO_4 laser. The amplifier increases the pulse energy to ~4 μJ at a repetition rate of 250 kHz (0.2 ps, 800 nm). These pulses are fed into an Optical Parametric Amplifier (OPA). In the OPA the beam is split: it is partially frequency-doubled and partially used to generate white light. Mixing of these beams leads to selective and tunable amplification of light at any selected wavelength in the range of 470 to 700 nm. This light can be used directly for excitation or after frequency doubling to 235–350 nm. Alternatively, the Ti:sapphire laser can be tuned in the range from 700 to 1000 nm and applying frequency doubling, this allows excitation at 'all' wavelengths longer than 235 nm. The excitation light is directed through a Berek variable waveplate to control its polarization direction and is focused into the sample by a lens of 15 cm focal length, leading to a focal spot of ~100 μm diameter.

B. Polarization

Anisotropic measurements can be performed in two ways: by adjusting the polarization of either the detected light, or the exciting light. In the first case one excites with vertically polarized light and turns a polarizer in the detection branch either horizontally of vertically, to obtain the perpendicular and parallel components of the emission. However, in this case one needs to correct for the difference in sensitivity of the detection system for horizontally and verti-

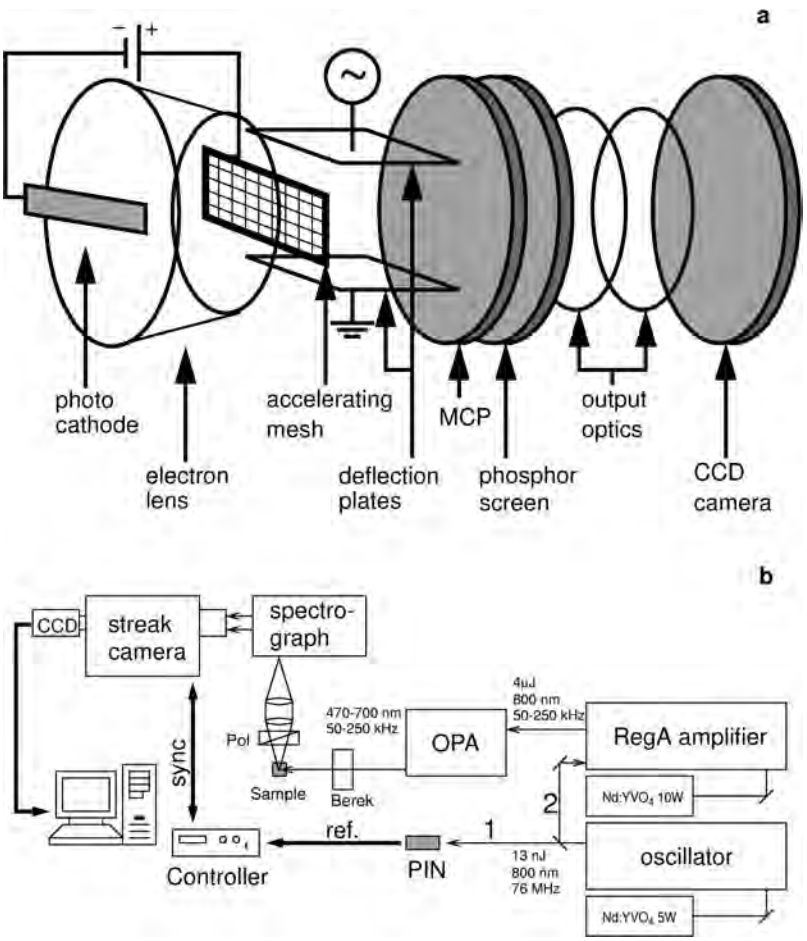

Fig. 2. Schematic representation of a streak camera (a) and of the synchroscan streak-camera setup (b). Further explanation in text.

cally polarized light. In particular the gratings of the spectrograph may introduce such a polarization-dependence of the sensitivity of the detection. The second way to record anisotropic measurements is by detecting only the vertical component of the emission, and using the Berek variable waveplate to turn the polarization of the excitation light to either horizontal or vertical, to obtain the perpendicular and parallel components of the emission. The advantage of this method is that one does not have to correct for the polarization-dependence of the detection, however, great care has to be taken not to move the excitation beam by adjusting the variable waveplate, since a change of the position of the focus in the sample will lead to unwelcome intensity changes. For isotropic measurements, one uses vertically polarized excitation light, and a detection polarizer set to the magic angle (54.74º). Finally, if the sample is contained in a rotating cell (see below) that is placed at an angle with the exciting light, one has to be aware that due to the refraction in the sample the direction of both the exciting light and the fluorescence is changed, which will affect both anisotropic and isotropic measurements.

C. Detection

Light following path 1 hits a reference diode, a tunnel diode, which as a consequence oscillates with a frequency forced to the repetition rate of the laser oscillator. The output of the tunnel diode is used to phase-lock the sweep frequency of the streak camera to the pulses of the laser oscillator. For timing stability on a timescale of minutes, cancellation of drift of the timing is necessary (Uhring et al., 2003). The deflection field is a sine function of time, with period 1/75.9 MHz = 13.2 ns. The controller can phase-shift the deflection field to move the relevant part of the

fluorescence decay into the time window recorded on the CCD camera. The controller can also change the amplitude of the signal to set the time range. In our setup four time-windows can be selected ranging from 180 ps to 2 ns. Instead of phase-locking the deflection field frequency to the frequency of the laser oscillator, like in this setup, the opposite is also feasible: the laser oscillator could be phase locked to the frequency of the streak camera, in a way similar to the way lasers are being synchronized to synchrotrons or free-electron lasers (Knippels et al., 1998).

Light from the sample is collected at right angle to the excitation beam through an achromatic lens and the detection polarizer, and focused by a second achromatic lens onto the input slit of a modified Czerny-Turner polychromator. This is equipped with a turret of three gratings with different blazing (spectral window 250 nm) which together span the wavelength range of 250–850 nm. Using concave mirrors after the slit the light is collimated towards the grating and after that the diffracted light is focused onto the photocathode, where the photons induce photo-electrons. These electrons are accelerated by an accelerating mesh and then deflected by the sweeping field. Since the amplitude and sign of the deflection field are functions of time (varying between +V and –V), the extent of deflection depends on the time of arrival of the photon at the photocathode. Only electrons traveling through a field between $+V_c$ and $-V_c$ (V_c = critical deflection field strength) reach the MCP, all other electrons are deflected too much. The electric field is within the detection range every half period of the oscillation frequency, with alternating field sweep direction, so the overall MCP signal is the sum of multiple forward and backward decay trace fragments. This is the so-called backsweep effect. The photons arriving during the backsweep contain information on longer-lived species.

D. Sample Cell

Stable fluorescent chromophores can be measured in a normal cuvette but photosynthetic samples usually require special measuring cells to prevent photo damage and/or a build-up of long-lived triplet or charge-separated states. We mention two types of cells that can be used to measure photosynthetic preparations: a flow-through cell, and a spinning cell. In the case a flow-cell is used, the solute is pumped through a 1 × 1 mm cuvette with a typical speed of 100 mL/min. Using a repetition rate of 250 kHz, the sample is hit by 15 pulses while passing the excitation spot.

In the case a spinning cell (diameter ~0.1 m, 20–50 Hz rotation) is used, also under the repetition rate of 250 kHz, the sample is hit by 1.5 pulses while passing the excitation spot. This allows for higher intensities and triplet (typical lifetimes µs-ms) build-up is easily avoided. However, the sample returns to the same position with a frequency of 50 Hz, so the build-up of longer-lived (>10 ms) species may still occur. Also the cell is not suitable for larger particles like thylakoid membranes, since the centrifugal forces will spin the particles to the rim of the cell.

E. Fundamental and Technical Limitations

First we will estimate the number of photons detected per laser shot, which is the motivation for synchroscan averaging. Then we will investigate the different sources of time broadening of the instrument response function (IRF), which ultimately result in an IRF width of about 1% of the selected time range.

1. Light Limitations

The detection with a streak camera in combination with a spectrograph (polychromator) puts an important restriction on the size of the illuminated spot of the sample. First of all the horizontal slit of the streak camera typically needs to be closed down to less than 100 µm in order to obtain an instrument response width of a few ps. Alternatively, a narrow width photocathode (70 µm) can be used. This restricts the spot from which fluorescence is collected vertically. The vertical slit of the spectrograph restricts the spot horizontally. In order to maintain good temporal resolution low dispersion gratings, typically 50 grooves/mm, must be used. In order to obtain the desired spectral resolution, also the entrance slit of the spectrograph must be closed down (for a 1/4-m spectrograph, with 50 grooves/mm the dispersion is ~60 nm/mm) (note that some imaging spectrographs enlarge the image of the entrance slit onto the output focal plane by 20%). Therefore, the spot in the sample that is monitored by the detection system typically has a diameter of 100 µm.

The spectrograph also dictates the light collection optics. Typically a numerical aperture of f/4 is used (f is the focal length of the spectrograph).

To get an idea of the best case performance we presume front face detection, of a concentrated sample (in practice detection under an angle of 90

degrees is used, which reduces the detection efficiency significantly). How much light can we get in and out of the small spot monitored in the sample?

For isotropic emission, f/4 optics collect < 0.5% of the emitted light. Given the restrictions imposed by the spot-sizes and slit-widths, deviating from 1:1 imaging of the fluorescence would not help, because a larger collection angle that can be attained would be spoiled by the magnification of the spot onto the entrance slit. Larger collection angles would require a spectrograph with a larger numerical aperture. This can be reached by using larger mirrors and gratings, but, as will become clear in Section II.E.2, the broadening in the spectrometer is proportional to the size of the beam inside the spectrometer. The other way to get a larger collection angle would be to use a shorter focal length spectrograph, but this would further reduce the spectral resolution. The saturation fluence for a laser dye is typically 1 mJ/cm^2, which corresponds to about 75 nJ for a 100 μm spot size. Of course this excitation density cannot be used in a proper fluorescence experiment (except when studying lasing phenomena) and one typically needs to stay at least one order of magnitude below this value. Things are even worse for most photosynthetic systems where annihilation and other non-linear effects can occur. To avoid these effects, we will make some estimates for 1 nJ excitation pulses. Around 500 nm this corresponds to 2.5*10^9 photons. If these are all absorbed, the initial fluorescence intensity will be ~2.5*10^5 photons/ps (assuming a strongly emitting molecule with a radiative lifetime of 10 ns). Less than 0.5% of these photons is collected using with f/4 optics, so we are left with ~10^3 photons/ps entering the slit of the spectrograph. The efficiency of the spectrograph is typically 10–50%, and the quantum yield of the photocathode of the streak camera is 1–20%, so this leaves us with about 1–100 photoelectrons per ps, spread out along the spectral axis.

This demonstrates that substantial averaging is required in order to get good spectro-temporal data, i.e., a large number of shots are required. This is where the main difference between single shot and synchroscan streak cameras comes to light. Single shot devices are optically triggered by the excitation laser and the deflection field is directly generated by a fast photoconductive switch. The maximal switching frequency of such a device is in the kHz range. In a synchroscan camera the deflection field is an oscillatory function synchronized to the repetition rate of the laser oscillator. Therefore, repetition rates up to 76 MHz (and of course sub harmonics of this frequency) can be employed. With a high repetition rate system like the RegA (250 kHz), fluorescence signals from laser dyes can be obtained within seconds, and emission data from less luminant samples in tens of minutes.

2. Time Resolution

Together with the electronic contribution of the setup, the major limitation to the time resolution (on the fastest time base) comes from the dispersion in the spectrograph. This phenomenon is related to pulse broadening in pulse stretchers/compressors (Martinez, 1987), and stems from the fact that after angular dispersion the wave front of a light pulse exhibits a tilt (with respect to the phase front) given by (Hebling, 1996):

$$\tan(\theta) = -\lambda \frac{\partial \alpha}{\partial \lambda} \tag{1}$$

where λ is the average wavelength of the light, and α the wavelength-dependent dispersion angle. This can be included in the grating equation

$$\alpha = \arcsin\left(\frac{m\lambda}{d} - \sin(\beta)\right) \tag{2}$$

in which m represents the order of diffraction (for all practical purposes ±1), β the angle of incidence, and d the grating constant. This gives

$$\tan(\theta) = -\lambda \frac{m}{d}\left(\frac{1}{\sqrt{1-\left(m\lambda/d - \sin(\beta)\right)^2}}\right) \tag{3}$$

In other work (Schiller and Alfano,1980; Wiessner and Staerk, 1993), the term between brackets is ignored, which corresponds with taking the phase velocity of the light instead of the group velocity. For the example given here the difference is insignificant, but this would not be the case for more dispersive gratings.

The total spatial stretch that occurs is $W\tan(\theta)$, where W represents the width of the beam after the grating. This is where the numerical aperture of the detection and spectrograph enter. For an 1/4 m spectrograph, with f/4 optics, W = ~5 cm, and for λ =

600 nm, $m = 1$, $\beta = 0$, and d=20 μm (50 grooves/mm), this amounts to a spread $\Delta_{dispersion}$ of 1.5 mm, which corresponds to a temporal spread of 5 ps. Therefore, even when using a 50 grooves/mm grating one needs to reduce the f-number of the spectrograph (or the light collection) to get a time response that is close to the limits of the electronic part as described below.

The time resolution limits of the streak camera itself are given by the spread in transit time of the photoelectrons in the streak tube. The transit time spread is mainly generated in the region near the photocathode where the electrons still have a relatively low speed (Zavoiski and Fanchenko, 1965; Bradley and New, 1974; Campillo and Shapiro, 1983). The resulting distribution of transit times has a half width of

$$\Delta\tau_c = m\frac{\Delta v}{eE} \tag{4}$$

where m and e are the mass and charge of the electron, Δv is the halfwidth of the initial photoelectron velocity distribution, and E is the field strength in the vicinity of the photo-cathode. Clearly it is important to have a high acceleration voltage near the photocathode, typically fields of ~10 kV/cm are used. For this extraction field a kinetic energy spread of 1 eV (a blue photon on a red-sensitive photocathode) would lead to a time spread of ~4 ps, which is significant when operating the streak camera on the fastest time base. Near the cut-off wavelength of the photocathode the energy spread becomes much smaller (and fortunately most fluorescence experiments are performed there), but in general there is a noticeable increase of the width of the instrument response when detecting blue photons.

For a higher time resolution higher extraction fields are required, but this comes at the cost of field emission (field induced dark current from the photocathode) and reduced reliability. Significantly higher pulsed extraction voltages can be used for single shot devices but this is not possible at the sweep rate of synchroscan streak cameras. Moreover, once below the 1 ps resolution other factors start to become limiting, like the quality of the imaging of the photocathode onto the MCP. Any aberrations of the electrostatic or electromagnetic electron lens (like the chromatic aberration $\Delta\tau_c$ caused by differences in electron speeds) will have adverse effects on the width of the instrument response.

The timing errors described here are independent. Therefore the error calculus for the total temporal instrument response width Δ becomes

$$\Delta^2 = (\Delta\tau_c)^2 + (\Delta_{imaging})^2 + (\Delta_{dispersion})^2 + (\Delta_{width})^2 \tag{5}$$

Where $\Delta_{imaging}$ is the imaging error due to the electrostatic or magnetic lenses, $\Delta_{dispersion}$ is the dispersion error, and Δ_{width} is the error due to the streak-slitwidth or the cathode width. At time bases larger than 400 ps $\Delta_{imaging}$ and Δ_{width} dominate. Imaging a 70 μm photocathode on a 7 mm wide CCD yields an IRF width of ≈1% of the time base used. At shorter time bases the contribution of the other two terms becomes appreciable, resulting in an IRF width of 3 ps (at 700 nm) for the 200 ps time base (which is 1.5%). At short wavelengths the IRF has broadened to 4 ps because of the larger $\Delta\tau_c$, see Fig. 3a. The broadening of the IRF (to 24 ps) with the 2.2 ns time base is clearly visible in Fig. 6.

F. Averaging and Correction of Images

Typically, the sample is excited with pulses of 0.2 ps FWHM at a repetition rate of 50–250 kHz, which is much lower than the laser oscillator frequency (typically 76 MHz). Synchroscan streak cameras are generally chosen for their ability to do signal integration over extended periods, in which case the time resolution will generally be limited by the drift between the laser and the camera clock. Often individual datasets contain internal tell-tales for absolute timing and of drift, e.g., Rayleigh or Raman scattering signals of the excitation pulse can be used to pin down the exact timing of the dataset. A fool-proof method for eliminating all sources of electronic drifts and jitter consists of directly illuminating a spot of the photocathode with the excitation pulse so as to obtain a fiducial, which is an absolute timing reference (Jaanimagi et al., 1986; Uhring et al., 2003). Using drift compensation electronics, up to 1000 seconds of accumulation on the CCD chip can be performed without significant deterioration of the temporal resolution. Typically, the full time and wavelength ranges are 200 ps and 250 nm, respectively. In the dark the CCD chip accumulates a dark current, which can be minimized by using a Peltier cooling element. Data must be corrected by subtracting the measured dark current contribution. The sensitivity of the entire detection system is quite strongly position dependent. In particular at the edges of the streak-image

the signal shows a pronounced drop. To account for this spatial variation of the sensitivity, streak images are divided by a shading image. This shading image consists of a streak image of the light emitted by a halogen lamp, which is directed into the spectrograph. This shading correction directly accounts for the sensitivity variation along the time-axis, since the intensity of the lamp is constant in time. For the sensitivity variation along the wavelength-axis the emission spectrum of the lamp has to be taken into account, which is done prior to the analysis of the data. Thus, the data is also corrected for the spectral sensitivity of the system.

Because of the limited wavelength resolution of the spectrograph (7 nm FWHM), the curvature-corrected and averaged images can be reduced to a matrix of ≈1000 points in time and 30–60 points in wavelength. In this same averaging step outliers (e.g., resulting from cosmic rays) can be removed. To deal with the small remaining drift after compensation multiple data sets can be collected. Instead of averaging e.g. 30 minutes and suffering from drift induced time broadening, it is better to collect six averages of 5 minutes and correct them for slow drift of time zero. Then, after scrutinous inspection, to check for trends like sample degradation, the series of images can be averaged. Figure 1 depicts a filled contour plot of the PS I trimer data derived from 48 traces between 625 and 785 nm, resulting from an average of 20 images, which will be globally analyzed below. Other visualizations of these data can be found in Gobets (2002).

G. Calibrations

Because of the sinusoidal nature of the deflection field, the 'time per pixel' is not a constant, but varies over time. For the shortest (200 ps) time range the time per pixel is practically constant (because the sinusoid is practically linear near the zero-crossing), but for longer time ranges the time per pixel varies significantly. Calibration of the time base can be done by fitting the train of imaged pulses from an etalon, to estimate a polynomial function that describes the time per pixel over the whole time base. Calibration of the wavelength axis can be done with the help of the lines of a calibration lamp, to estimate a linear function. Images of continuous narrow-band sources are also instrumental for checking that the sweep axis is parallel to the vertical axis of the CCD. A crucial procedure for the analysis of the two-dimensional data sets is the characterization of the curvature of the image, i.e., the spatial dependence of 'time zero' on the CCD image, caused by the different path lengths of the photo-electrons in the streak camera. Additionally, the light-collecting optics and the spectrograph cause wavelength-dependent temporal shifts. To assess this curvature, scattering of the white light from the OPA is recorded with the streak camera, resulting in an IRF limited curved line on the streak image. In its turn, the intrinsic dispersion of the white light itself is measured using the optical Kerr signal in carbon disulphide (Greene and Farrow, 1983). The combination of both these measurements yields the spatial dependence of time zero during a measurement.

H. Further Exploitation of the Horizontal Dimension

Streak tubes generally contain a second set of deflection plates, to facilitate the horizontal deflection of photoelectrons. In commercial instruments these plates are used, e.g., for blanking (blocking) the detection in between sweeps, or during the back sweep of the camera. These horizontal plates can also be exploited to perform 2D experiments other than the ones we focused on above, and consequently, spectral information will be lost. In Buhler et al. (1998) and Ohtani et al. (1999) the horizontal sweep plates were used to provide a secondary, slow, time axis. In combination with a stopped-flow apparatus, the time-evolution of the ps fluorescence lifetime of a sample could thus be measured on a ms time scale. In van Mourik et al. (2003) the horizontal sweep direction was synchronized to the electric field applied in a Stark fluorescence experiment, and thus the effect of the Stark field on the fluorescence intensity and lifetime of the sample could be measured.

III. Data Analysis

When the streak image has been corrected for the instrumental curvature it is ready for data analysis. The aim is to obtain a model-based description of the full data set in terms of a model containing a small number of precisely estimated parameters, of which the rate constants and spectra are the most relevant. With polarized-light experiments also anisotropy parameters come into play. Description of the basic ingredient of kinetic models, the exponential decay, will be given first, followed by a description of how

to use these ingredients for global and target analysis (for reviews, see Holzwarth, 1996 and van Stokkum et al., 2004) of the full data. Our main assumption here is that the time and wavelength properties of the system of interest are separable, which means that spectra of species or states are constant. For details on parameter estimation techniques the reader is also referred to the above cited reviews and references cited therein, and to van Stokkum (2005). Software issues are discussed in van Stokkum and Bal (2006). We will describe in depth the analysis of typical streak data, with the analysis of the PS I trimer data serving as the main example.

A. Modeling an Exponential Decay

Here an expression is derived for describing the contribution of an exponentially decaying component to the streak image. The instrument response function (IRF) $i(t)$ can usually adequately be modeled with a Gaussian with parameters μ and Δ for, respectively, location and full width at half maximum (FWHM):

$$i(t) = \frac{1}{\tilde{\Delta}\sqrt{2\pi}} \exp(-\log(2)(2(t-\mu)/\Delta)^2) \tag{6}$$

where $\tilde{\Delta} = \Delta / (2\sqrt{2\log(2)})$. The adequacy of the Gaussian approximation of the IRF shape is depicted in Fig. 3a. The convolution (indicated by an *) of this IRF with an exponential decay (with rate k) yields an analytical expression which facilitates the estimation of the IRF parameters μ and Δ:

$$\begin{aligned} c(t,k,\mu,\Delta) &= \exp(-kt) * i(t) \\ &= \frac{1}{2}\exp(-kt)\exp\left(k\left(\mu + k\tilde{\Delta}^2/2\right)\right)\left\{1+\operatorname{erf}\left(\frac{t-(\mu+k\tilde{\Delta}^2)}{\sqrt{2}\tilde{\Delta}}\right)\right\} \end{aligned} \tag{7}$$

The periodicity of the synchroscan results in detection of the fluorescence that remains after multiples of half the synchroscan period T (typically T≈13 ns). Therefore, if lifetimes longer than ~1 ns occur in a sample, the above expression should be extended with a summation over the signal contributions that result from forward and backward sweeps:

$$\begin{aligned} c(t,k,T) &= \sum_{n=0}^{\infty} e^{-kTn}\left(e^{-k(t-\mu+T)} + e^{-k(T/2-t-\mu)}\right) \\ &= \left(e^{-k(t-\mu+T)} + e^{-k(T/2-t-\mu)}\right) \Big/ \left(1-e^{-kT}\right) \end{aligned} \tag{8}$$

Note that it is assumed here that time zero of the time base corresponds to the zero crossing of the sweep, and that the convolution with the IRF is no longer necessary at times longer than $T/2$. Adding the previous expressions provides the full model function for an exponential decay recorded with a synchroscan streak camera and will henceforth be denoted by $c^l(k)$:

$$c^l(k) \equiv c(t,k,\mu,\Delta,T) = c(t,k,\mu,\Delta) + c(t,k,T) \tag{9}$$

Examples of $c^l(k)$ are depicted in Fig. 4c, and fits of traces with linear combinations of decays are shown in Fig. 3b, where an ultrafast lifetime of 1.2 ps is detected, and Fig. 3c, which is dominated by a 17 ns lifetime (note the huge backsweep signal apparent from the signal 'before time zero'). Figure 4a and b depict the fits of two traces from the data shown in Fig. 1, using 5 lifetimes. The simultaneous estimation of up to 5 lifetimes in the range of (sub)ps to ns is more or less routine.

Because fluorescence samples are relatively dilute, elastic scattering or Raman scattering of the excitation light by water (or of other solvents) can complicate the measurement, if they occur within the analyzed wavelength interval. Such contributions can be modeled with an extra component with a time course identical to the IRF $i(t)$. Usually it is possible to restrict the contribution of scattering to a limited wavelength region.

If the streak image has not been corrected for the instrumental curvature the wavelength dependence of the IRF location μ can be modeled with a polynomial (usually a parabola is adequate). Sometimes the IRF shape is better described by a superposition of two Gaussians, leading to a superposition description of the exponential decay (van Stokkum, 2005).

B. Global and Target Analysis

The basis of global analysis is the superposition principle, which states that the measured data $\psi(t,\lambda)$ result from a superposition of the spectral properties $\varepsilon_l(\lambda)$ of the components present in the system of interest

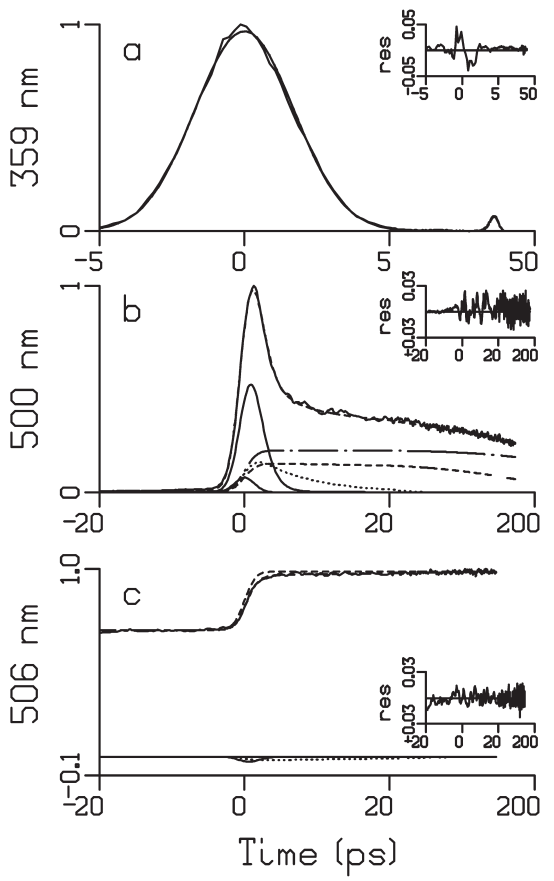

Fig. 3. (a) IRF of streak scope measured from scattered white light fitted with a Gaussian. Estimated FWHM Δ = 4 ps, note a small (7%) reflection after 26 ps. Detection wavelength (in nm) indicated along the ordinate. Dashed lines indicate fit. Insets show residuals. Note that the time axis is linear from –5 to +5 ps relative to the maximum of the IRF, and logarithmic thereafter. In (b) and (c) it is linear from –20 to +20 ps. (b) Emission from thioredoxin reductase mutant C138S (from van den Berg et al., 2001) showing a dominant 1.2 ps decay (depicted by solid line). Other contributions to the fit have lifetimes of 7.3 ps (dotted), 0.18 ns (dashed), 0.74 ns (dot dashed), and pulse follower (chain dashed). The sum of these contributions which is the fit of the trace is shown as a dashed line. (c) Emission from lumazine protein (from Petushkov et al., 2003) showing a dominant 17 ns decay (depicted by dashed line). Other contributions to the fit have lifetimes of 0.7 ps (solid) and 24 ps (dotted).

weighted by their concentration $c_l(t)$,

$$\psi(t,\lambda) = \sum_{l=1} c_l(t)\varepsilon_l(\lambda) \qquad (10)$$

The $c_l(t)$ of all n_{comp} components are described by a compartmental model, that consists of first-order differential equations, with as solution sums of exponential decays. We will consider three types of compartmental models: (1) a model with components decaying mono-exponentially in parallel, which yields Decay Associated Spectra (DAS), (2) a sequential model with increasing lifetimes, also called an unbranched unidirectional model, giving Evolution Associated Spectra (EAS), and (3) a full compartmental scheme which may include possible branchings and equilibria, yielding Species Associated Spectra (SAS). The latter is most often referred to as target analysis, where the target is the proposed kinetic scheme, including possible spectral assumptions.

(1) With parallel decaying components the model reads:

$$\psi(t,\lambda) = \sum_{l=1}^{n_{comp}} c^I(k_l) DAS_l(\lambda) \qquad (11)$$

The DAS thus represent the estimated amplitudes of the above defined exponential decays $c^I(k_l)$. The DAS estimated from the PS I trimer data are shown in Fig. 4d. Several observations can be made: the 0.4 ps DAS (solid) represents the rise due to the relaxation from the initially excited Soret state (a higher excited state, of which the emission is outside the detection range) to the Q_y emission (lowest excited state). The next DAS of 3.9 ps (dotted) is conservative, i.e., the positive and negative areas are more or less equal. It represents decay of more blue and rise of more red emission, and can be interpreted as energy transfer from bulk to red chlorophyll *a* (Chl *a*), i.e. Chl *a* that absorb at wavelengths longer than the primary electron donor P700. The 15 ps DAS (dashed) is not conservative, although it does show some rise above 730 nm. Apparently some trapping of excitations takes place on this time scale, concurrently with energy transfer. The 50 ps DAS (dot dashed) represents the trapping spectrum. The long lived (4.9 ns) DAS (chain dashed) is attributed to a small fraction of free Chl *a* in the preparation. Clearly, the first three DAS do not represent pure species, and they are interpreted as linear combinations (with positive and negative contributions) of true species spectra.

(2) A sequential model reads:

$$\psi(t,\lambda) = \sum_{l=1}^{n_{comp}} c_l^{II} EAS_l(\lambda) \qquad (12)$$

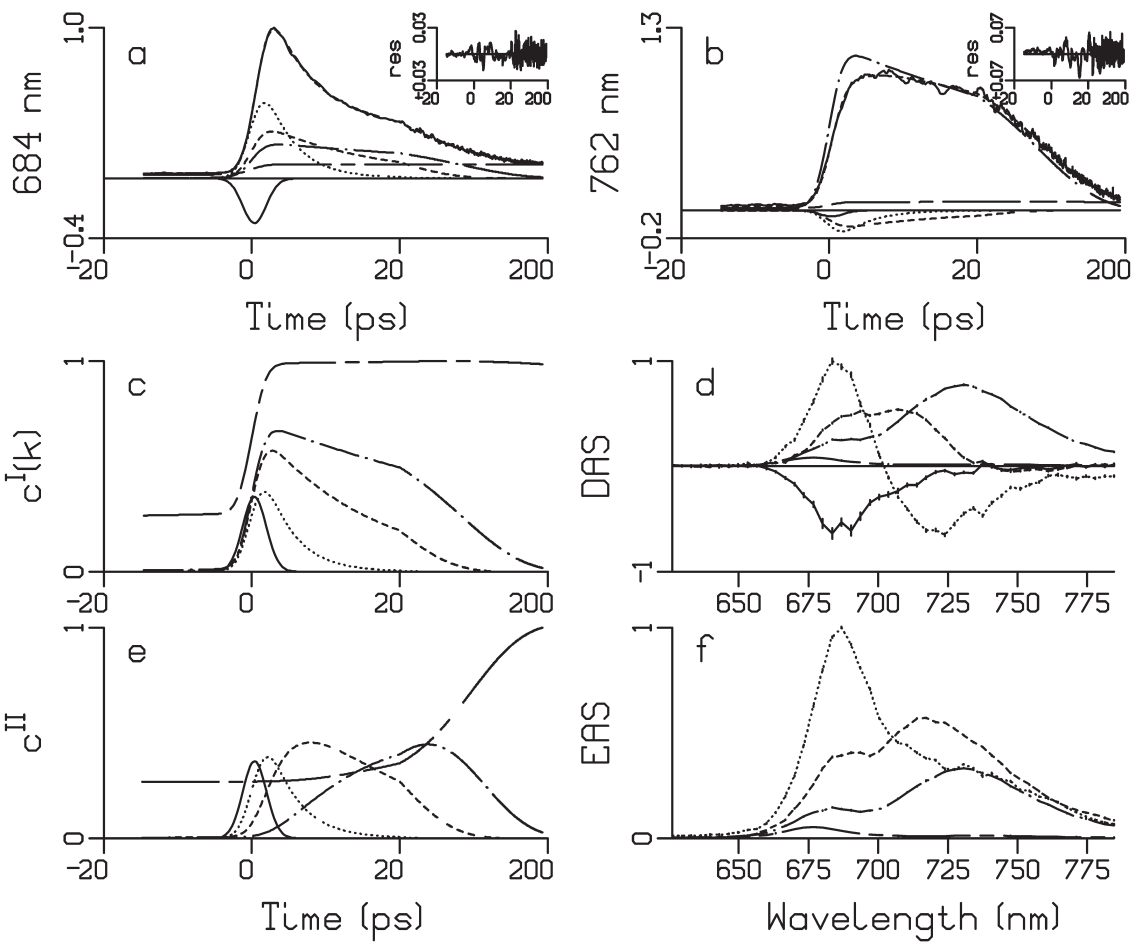

Fig. 4. Results from global analysis of PS I data depicted in Fig. 1. Note that in a–c and e the time axis is linear from –20 to +20 ps relative to the maximum of the IRF, and logarithmic thereafter. Insets in a, b show residuals. (a) Fit of bulk Chl *a* emission trace showing multiexponential decay. Contributions of the five exponential decays with different lifetimes (shown in c) are indicated by line type. (b) Fit of red Chl *a* emission trace showing multiexponential rise and decay. (c) Exponential decays $c^I(k_l)$. Estimated lifetimes: 0.4 ps (solid), 3.9 ps (dotted), 15 ps (dashed), 50 ps (dot dashed), and 4.9 ns (chain dashed). (d) Decay Associated Spectra (DAS), note that the first DAS which represents overall rise has been multiplied by 0.2. Vertical bars indicate estimated standard errors. (e) Evolutionary concentration profiles c^{II} (assuming a sequential kinetic scheme with increasing lifetimes). (f) Evolution Associated Spectra (EAS). Note that the first EAS is zero, since excitation was in the Soret band.

where each concentration is a linear combination of the exponential decays,

$$c_l^{II} = \sum_{j=1}^{l} b_{jl} c^I(k_l) \qquad (13)$$

and the amplitudes b_{jl} are given by $b_{11} = 1$ and for $j \le l$:

$$b_{jl} = \frac{\prod_{m=1}^{l-1} k_m}{\prod_{n=1, n\neq j}^{l} \left(k_n - k_j\right)} \qquad (14)$$

Examples of c^{II} are depicted in Fig. 4e, whereas the EAS estimated from the PS I trimer data are shown in Fig. 4f. With increasing lifetimes, and thus decreasing rates k_l, the first EAS (equal to the sum of DAS) corresponds to the spectrum at time zero with an ideal

infinitely small IRF, $i(t) = \delta(t)$. In Fig. 4f, this first EAS is zero in the Q_y region. The second EAS (dotted), which is formed in 0.4 ps and decays in 3.9 ps, represents the sum of the spectra of all excitations that have arrived from the Soret region, and is dominated by bulk Chl *a*. The third EAS, which is formed in 3.9 ps and decays in 15 ps, is already dominated by red Chl *a* emission, which is even more the case with the fourth EAS (dot dashed, formed in 15 ps, decays in 50 ps). The final EAS (chain dashed, formed in 50 ps) is proportional to the final DAS, and represents the spectrum of the longest living component (4.9 ns). Clearly, these EAS do not represent pure species, except for the final EAS, and they are interpreted as a weighted sum (with only positive contributions) of true species spectra.

(3) When neither of these two simple models is applicable, a full kinetic scheme may be appropriate. The problem with such a scheme is that, while the kinetics are described by microscopic rate constants, the data only allows for the estimation of decay rates (or lifetimes). Thus additional information is required to estimate the microscopic rates, which can be spectral constraints (zero contribution of SAS at certain wavelengths) or spectral relations. This is explained in detail in van Stokkum et al. (2004).

Now the model reads:

$$\psi(t,\lambda) = \sum_{l=1}^{n_{comp}} c_l^{III} SAS_l(\lambda) \qquad (15)$$

where the concentrations c_l^{III} are again linear combinations of the exponential decays, with coefficients that depend upon the microscopic rate constants that describe the transitions between all the compartments. Figure 5a depicts the kinetic scheme that was applied to the trimeric PS I data of Fig. 1. The concentrations of all compartments are collated in a vector $c(t) = [c_1(t)\ c_2(t)\ \ldots\ c_{n\_c}(t)]^T = [S(t)\ B(t)\ R_1(t)\ R_2(t)\ F(t)]^T$, which obeys the differential equation:

$$\frac{d}{dt}c(t) = Kc(t) + j(t) \qquad (16)$$

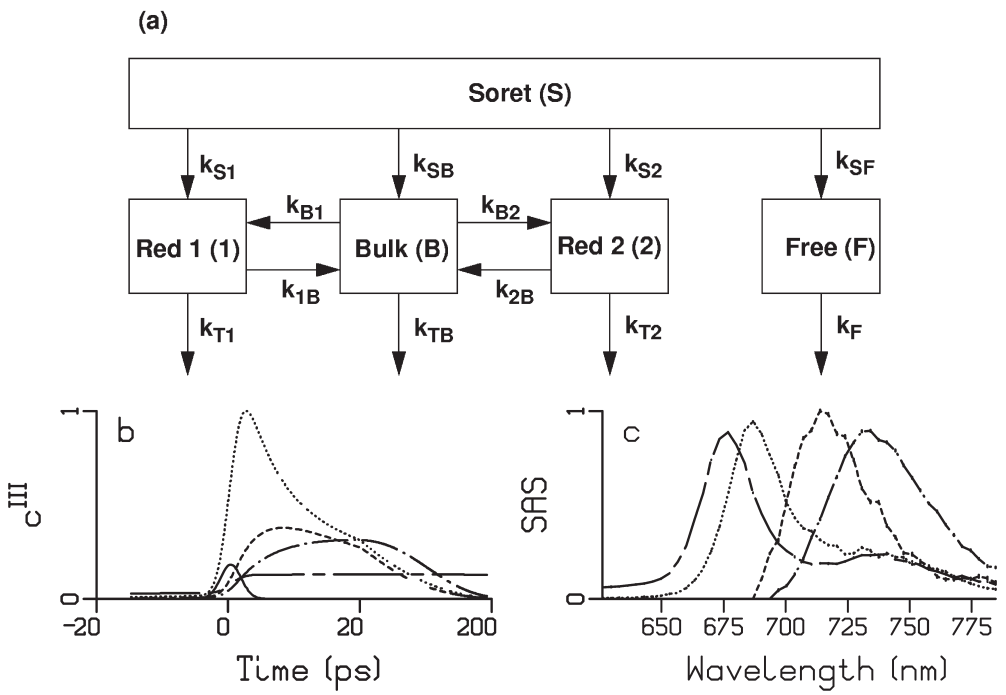

Fig. 5. (a) Kinetic scheme used for the target analysis of PS I data depicted in Fig. 1. After excitation in the Soret band four compartments are populated: bulk Chl *a* (B), two pools of red Chl *a* (1 and 2) and a small fraction of free Chl *a* (F). The first three compartments equilibrate, and excitations are trapped with different rates. (b) Concentration profiles c_l^{III}. Note that the time axis is linear from –20 to +20 ps relative to the maximum of the IRF, and logarithmic thereafter. (c) Species Associated Spectra (SAS). Key in (b) and (c): bulk Chl *a* (dotted), red Chl *a* 1 (dashed), red Chl *a* 2 (dot dashed), free Chl *a* (chain dashed).

where the transfer matrix K contains off-diagonal elements k_{pq}, representing the microscopic rate constant from compartment p to compartment q. The diagonal elements contain the total decay rates of each compartment. The input to the compartments is $j(t) = i(t)[1\ 0\ 0\ 0\ 0]^T$. The K matrix from Fig. 5a reads:

$$K = \begin{bmatrix} -(k_{SB}+k_{S1}+k_{S2}+k_{SF}) & & & & \\ k_{SB} & -(k_{TB}+k_{B1}+k_{B2}) & k_{1B} & k_{2B} & \\ k_{S1} & k_{B1} & -(k_{T1}+k_{1B}) & & \\ k_{S2} & k_{B2} & & -(k_{T2}+k_{2B}) & \\ k_{SF} & & & & -k_F \end{bmatrix} \tag{17}$$

In Fig. 5b, the c [illegible] ve been drawn, calculated from the estimated parameters, whereas the estimated SAS are shown in Fig. 5c. Note that it has been assumed that the two red Chl *a* compartments only contribute above 690 and 697 nm, respectively. Therefore, the forward and backward rate constants between the bulk Chl *a* compartment and both compartments of red Chl *a* can be estimated from the multi-exponential decay of the bulk Chl *a*. The SAS in Fig. 5c are considered satisfactory, because the shapes of the bulk and red SAS resemble the free Chl *a* SAS, and the areas, and thus the oscillator strengths, of the different Chls *a* are equal within 10%. This area constraint was instrumental in determining the branching ratios from Soret to the four different Chl *a* pools, and the trapping ratios.

1. Target Analysis of Anisotropic Data

When in addition to magic angle (MA) data also parallel (VV) and perpendicular (VH) data are collected, more information is available to disentangle the complex kinetics, and estimate the SAS. In such an extended target analysis the magic angle concentrations c^{III}_l are multiplied by the anisotropic properties of the components.

$$\begin{bmatrix} MA(t,\lambda) \\ VV(t,\lambda) \\ VH(t,\lambda) \end{bmatrix} = \sum_{l=1}^{n_{comp}} c_l^{III} SAS_l(\lambda) \begin{bmatrix} 1 \\ 1+2r_l \\ 1-r_l \end{bmatrix} \tag{18}$$

Note that here the anisotropy r_l is assumed to be constant. When an anisotropy decay rate is present, each isotropic exponential decay has to be multiplied by the associated anisotropy decay rate before the convolution with the IRF (Beechem 1989; Yatskou et al., 2001). Figure 6 shows a representative trace

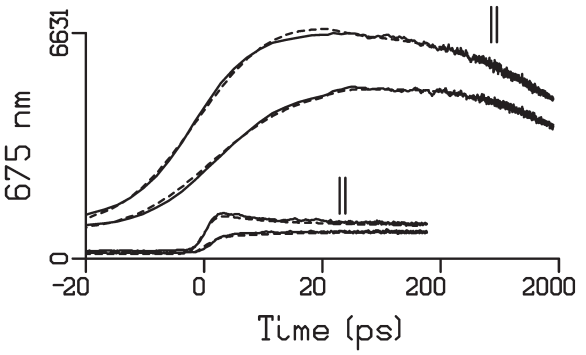

Fig. 6. Parallel (||, upper curves) and perpendicular (lower curves) time traces measured at 675 nm after exciting PCP at 660 nm, from Kleima et al. (2000). The smaller curves were measured on the shortest time base. The dashed lines indicate the fit. Note that the time axis is linear from –20 to +20 ps relative to the maximum of the IRF, and logarithmic thereafter.

from Kleima et al. (2000) who used a bi-exponential anisotropy decay

$$r(t) = A_1 \exp(-t/\tau_1) + A_2 \exp(-t/\tau_2) + r_\infty \tag{19}$$

An isotropic lifetime of ≈4.2 ns was estimated from this target analysis, in combination with depolarization times of about 7 and 350 ps, which are clearly visible in the data measured on the different time scales.

C. Spectral Modeling

SAS can sometimes be fitted with a spectral model consisting of a skewed Gaussian in the energy domain ($\bar{\nu} = 1/\lambda$):

$$SAS(\bar{\nu}) = \bar{\nu}^5 S_{\max} \exp\left(-\ln(2)\{\ln(1+2b(\bar{\nu}-\bar{\nu}_{\max})/\Delta\bar{\nu})/b\}^2 \right) \tag{20}$$

where the parameter $\bar{\nu}_{max}$ is the Franck-Condon wavenumber of maximum emission. The FWHM is given by $\Delta\bar{\nu}_{1/2} = \Delta\bar{\nu}\ \sinh(b)/b$. Note that with skewness parameter b equal to zero the expression simplifies to a Gaussian. The average wavenumber of this function is given by

$$\bar{\nu}_{av} = \bar{\nu}_{\max} + \frac{\Delta\bar{\nu}}{2b}\left(\exp\left(-3b^2 \Big/ 4\ln(2) \right) - 1 \right) \tag{21}$$

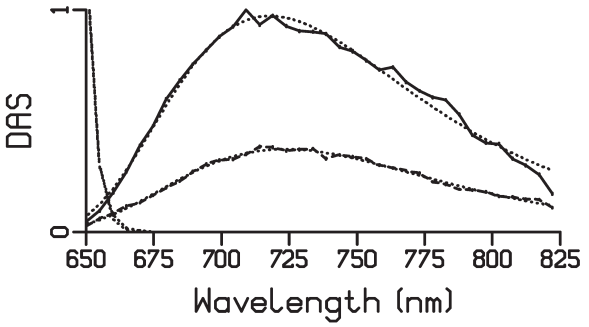

Fig. 7. Decay Associated Spectra from global analysis of bacteriorhodopsin mutant D85S excited at 635 nm, from van Stokkum et al. (2006). Key: 5.2 ps (solid), 19.1 ps (dashed), scatter (dotted). Fits of the DAS using a skewed Gaussian shape are indicated by dots. The estimated $\bar{\nu}_{av}$ were both 13000 cm^{-1} and the FWHM was 2540 cm^{-1}.

The spectral evolution description of solvation approximates a gradual change with an average spectral change associated with a time constant. Alternatively, solvation occurring on sub-ps timescales can be described using a time-dependent shift of $\bar{\nu}_{max}$ (Horng et al., 1995; Vilchiz et al., 2001). This requires data with a higher time and wavelength resolution, e.g. from fluorescence up-conversion (Horng et al., 1995; Pal et al., 2002; Vengris et al., 2004), for which excitation intensities are required that are too high for the study of photosynthetic systems.

Figure 7 shows DAS estimated from the multi-exponential decay of the excited state of the D85S mutant of bacteriorhodopsin. Both DAS possessed almost identical shapes, and thus show no evidence for solvation on the picosecond timescale. The DAS were well described by a skewed Gaussian, and the multi-exponentiality is ascribed to heterogeneity of the protein.

D. Usage of the Singular Value Decomposition

The matrix structure of the streak data enables the usage of matrix decomposition techniques, in particular the singular value decomposition (SVD). Formally the data matrix can be decomposed as

$$\psi(t,\lambda) = \sum_{l=1}^{m} u_l(t) s_l w_l(\lambda) \tag{22}$$

Where u_l and w_l are the left and right singular vectors, s_l the sorted singular values, and m is the minimum of the number of rows and columns of the data matrix. The singular vectors are orthogonal, and provide an optimal least squares approximation of the matrix.

From the SVD the rank of the data matrix can be estimated, as judged from the singular values and singular vector pairs significantly different from noise. This rank corresponds to the number of spectrally and temporally independent components. When the

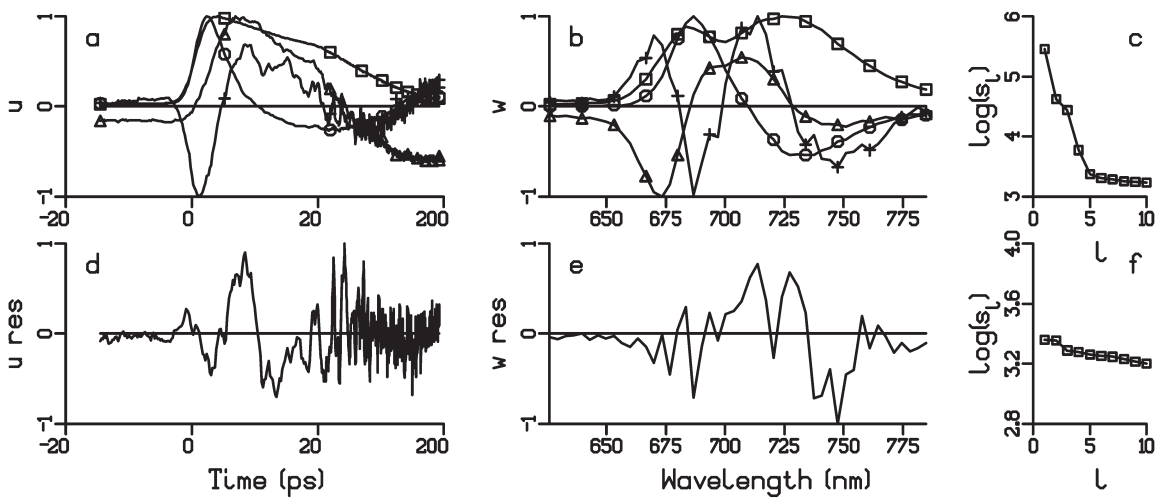

Fig. 8. SVD of the PS I trimer data matrix (top) and matrix of residuals (bottom). (a) First four (order squares, circles, triangles, plus symbols) left singular vectors u_l, (b) first four right singular vectors w_l, (c) first ten singular values s_l on a logarithmic scale, (d) first left singular vector $u_{res,1}$, (e) first right singular vector $w_{res,1}$, (f) first ten singular values $s_{res,1}$ on a logarithmic scale.

data matrix has not been corrected for dispersion, this is no longer true. Furthermore SVD of the residual matrix is useful to diagnose shortcomings of the model used, or systematic errors in the data. Figure 8a-c depicts the SVD of the trimeric PS I data, where four singular values and singular vector pairs are significantly different from noise. These first four singular values account for 99.923% of the variance of the data matrix. The left and right singular vectors are both linear combinations of the true concentration profiles and SAS, and are hard to interpret. The first pair (squares) represents a kind of average. The SVD of the residual matrix (shown in Fig. 8d-f) shows that its singular values are comparable to the noise singular values in Fig. 8c, and that there is no clear structure in the first singular vector pair. The sum of squares of the residuals is 0.088% of the variance of the data matrix, indicating a small lack of fit. The root mean square error of the fit was 41, which is 0.5% of the peak in Fig. 1.

IV. Conclusions

When comparing the present state of the art with the excellent review of Campillo and Shapiro (1983) the most striking developments are the utilization of the horizontal dimension, in particular using a spectrograph, and the improvement of the data analysis methods. The collection and analysis of true spectro-temporal measurements with (sub)ps time resolution using low excitation intensities have become routine, and the promises of the technique have largely been fulfilled. It has now become possible to functionally describe the complicated energy transfer and trapping processes in photosynthetic complexes with the help of a compartmental model, characterized by SAS and microscopic rate constants. The streak measurements of spectral evolution of fluorescence can be combined with fluorescence up-conversion measurements (Gobets et al., 2001a; Kennis et al., 2001) to extend the number of time scales covered, or with femtosecond difference absorption measurements (Groot et al., 2005) to uncover also non-emitting states. The complementary information contained in data obtained with different techniques is optimally extracted in a simultaneous target analysis.

Acknowledgments

Marloes Groot, Kate Mullen, Arie van Hoek, Janne Ihalainen and Rienk van Grondelle are thanked for critically reading the text. This research was supported by the Netherlands Organization for Scientific Research (NWO) via the Dutch Foundation of Earth and Life Sciences (ALW) and via the Netherlands Organization of Fundamental Research of Matter (FOM).

References

Andrizhiyevskaya EG, Frolov D, van Grondelle R, and Dekker JP (2004a) Energy transfer and trapping in the Photosystem I complex of *Synechococcus* PCC 7942 and in its supercomplex with IsiA. Biochim Biophys Acta 1656: 104–113

Andrizhiyevskaya EG, Frolov D, van Grondelle R, and Dekker JP (2004b) On the role of the CP47 core antenna in the energy transfer and trapping dynamics of Photosystem II. Phys Chem Chem Phys 6: 4810–4819

Beechem JM (1989) A second generation global analysis program for the recovery of complex inhomogeneous fluorescence decay kinetics. Chem Phys Lipids 50: 237–251

Bradley DJ and New GHC (1974) Ultrashort pulse measurements. Proc IEEE 62: 313–345

Buhler CA, Graf U, Hochstrasser RA and Anliker M (1998) Multidimensional fluorescence spectroscopy using a streak camera based pulse fluorimeter. Rev Sci Instrum 69: 1512–1518

Campillo AJ and Shapiro SL (1983) Picosecond streak camera fluorometry — a review. IEEE J Quantum Electron QE-19: 585–603

Donovan B, Walker LA, Kaplan D, Bouvier M, Yocum CF and Sension RJ (1997) Structure and function in the isolated reaction center complex of Photosystem II. I. Ultrafast fluorescence measurements of PS II. J Phys Chem B 101: 5232–5238

Fleming GR, Morris JM and Robinson GW (1977) Picosecond fluorescence spectroscopy with a streak camera. Austr. J. Chem. 30: 2338–2352

Freiberg A and Saari P (1983) Picosecond spectrochronography. IEEE J Quantum Electron QE-19: 622–630

Gilmore AM, Itoh S and Govindjee (2000) Global spectral-kinetic analysis of room temperature chlorophyll *a* fluorescence from light-harvesting antenna mutants of barley. Phil Trans R Soc Lond B 355: 1371–1384

Gilmore AM, Matsubara S, Ball MC, Barker DH and Itoh S (2003a) Excitation energy flow at 77 K in the photosynthetic apparatus of overwintering evergreens. Plant Cell Environ 26: 1021–1034

Gilmore AM, Larkum AWD, Sallh A, Itoh S, Shibata Y, Bena C, Yamasaki H, Papina M and Woesik R (2003b) Simultaneous time resolution of the emission spectra of fluorescent proteins and zooxanthellar chlorophyll in reef-building coral. Photochem Photobiol 77: 515–523

Greene BJ and Farrow RC (1983) The subpicosecond Kerr effect in CS_2. Chem Phys Lett 98: 273–276

Gobets B (2002) The life and times of Photosystem I. Excita-

tion energy transfer and trapping unravelled. Thesis, Vrije Universiteit Amsterdam

Gobets B, Kennis JTM, Ihalainen JA, Brazzoli M, Croce R, van Stokkum IHM, Bassi R, Dekker JP, van Amerongen H, Fleming GR and van Grondelle R (2001a) Excitation energy transfer in dimeric Light Harvesting Complex I: A combined streak-camera/fluorescence upconversion study. J Phys Chem B 105: 10132–10139

Gobets B, van Stokkum IHM, Rögner M, Kruip J, Schlodder E, Karapetyan N, Dekker JP and van Grondelle R (2001b) Time-resolved fluorescence emission measurements of Photosystem I particles of various cyanobacteria: A unified compartmental model. Biophys J 81: 407–424

Gobets B, van Stokkum IHM, van Mourik F, Dekker JP and van Grondelle R (2003) Excitation wavelength dependence of the fluorescence kinetics in Photosystem I particles from *Synechocystis* PCC 6803 and *Synechococcus elongatus*. Biophys J 85: 3883–3898

Groot ML, Pawlowicz NP, van Wilderen LJGW, Breton J, van Stokkum IHM, and van Grondelle R (2005) Initial electron donor and acceptor in isolated Photosystem II reaction centers identified with femtosecond mid-IR spectroscopy. Proc Natl Acad Sci USA 102: 13087–13092

Haacke S, Vinzani S, Schenkl S and Chergui M (2001) Spectral and kinetic fluorescence properties of native and nonisomerizing retinal in bacteriorhodospin. Chem Phys Chem 2: 310–315

Hebling J (1996) Derivation of the pulse front tilt caused by angular dispersion, Opt Quantum Electron 28: 1759–1763

Holzwarth AR (1996) Data analysis of time-resolved measurements. In: Amesz J and Hoff AJ (eds) Biophysical Techniques in Photosynthesis (Advances in Photosynthesis and Respiration, Vol. 3), pp 75–92. Kluwer Academic Press, Dordrecht.

Horng ML, Gardecki JA, Papazyan A and Maroncelli M (1995) Subpicosecond measurements of polar solvation dynamics: Coumarin 153 revisited. J Phys Chem 99: 17311–17337

Ihalainen JA, Jensen PE, Haldrup A, van Stokkum IHM, van Grondelle R, Schneller HV and Dekker JP (2002) Pigment organization and energy transfer dynamics in isolated Photosystem I (PS I) complexes from *Arabidopsis thaliana* depleted of the PS I-G, PS I-K, PS I-L or PS I-N subunit. Biophys J 83: 2190–2201

Ihalainen JA, Croce R, Morosinotto T, van Stokkum IHM, Bassi R, Dekker JP, van Grondelle R (2005a) Excitation decay pathways of Lhca proteins – A time-resolved fluorescence study. J Phys Chem B 109: 21150–21158

Ihalainen JA, D'Haene S, Yeremenko N, van Roon H, Arteni AA, Boekema EJ, van Grondelle R, Matthijs HCP, and Dekker JP (2005b) Aggregates of the chlorophyll-binding protein IsiA (CP43′) dissipate energy in cyanobacteria. Biochemistry 44: 10846–10853

Ihalainen JA, Klimmek F, Ganeteg U, van Stokkum IHM, van Grondelle R, Jansson S, and Dekker JP (2005c) Excitation energy trapping in Photosystem I complexes depleted in Lhca1 and Lhca4. FEBS Lett 579: 4787–4791

Ihalainen JA, van Stokkum IHM, Gibasiewicz K, Germano M, van Grondelle R and Dekker JP (2005d) Kinetics of excitation trapping in intact Photosystem I of *Chlamydomonas reinhardtii* and *Arabidopsis thaliana*. Biochim Biophys Acta 1706: 267–275

Ito T, Hiramatsu M, Hosoda M and Tsuchiya Y (1991) Picosecond time-resolved absorption spectrometer using a streak camera. Rev Sci Instrum 62: 1415–1419

Jaanimagi PA, DaSilva L, Gregory GG, Hestdalen C, Kiikka CD, Kotmel R, and Richardson MC (1986) Optical fiducials for X-ray streak cameras at LLE. Rev Sci Instrum 57: 2189–2191

Jimenez R and Fleming GR (1996) Ultrafast spectroscopy of photosynthetic systems. In: Amesz J and Hoff AJ (eds) Biophysical Techniques in Photosynthesis (Advances in Photosynthesis and Respiration, Vol 3), pp 63–73. Kluwer Academic Press, Dordrecht

Kamiya N, Ishikawa M, Kasahara K, Kaneko M, Yanamoto N and Ohtani H (1997) Picosecond fluorescence spectroscopy of the purple membrane of *halobacterium halobium* in alkaline suspension. Chem Phys Lett 265: 595–599

Kennis JTM, Gobets B, van Stokkum IHM, Dekker JP, van Grondelle R and Fleming GR (2001) Light harvesting by chlorophylls and carotenoids in the Photosystem I core complex of *Synechococcus elongates*: A fluorescence upconversion study. J Phys Chem B 105: 4485–4494

Kleima FJ, Hofmann E, Gobets B, van Stokkum IHM , van Grondelle R, Diederichs K and van Amerongen H (2000) Förster excitation energy transfer in peridinin-chlorophyll-*a*-protein. Biophys J 78: 344–353.

Knippels GMH, van de Pol MJ, Pellemans HPM, Planken PCM, and van der Meer AFG (1998) Two-color facility based on a broadly tunable infrared free-electron laser and a subpicosecond-synchronized 10-fs-Ti:Sapphire laser. Opt Lett 23: 1754–1756

Krishnan RV, Saitoh H, Terada H, Centonze VE and Herman B (2003) Development of a multiphoton fluorescence lifetime imaging microscopy system using a streak camera. Rev Sci Instrum 74: 2714–2721.

Lin S and Knox RS (1988) Time resolution of a short-wavelength chloroplast fluorescence component at low temperature. J Lumin 40/41: 209–210.

Lin S and Knox RS (1991) Studies of excitation-energy transfer within the green-alga *Chlamydomonas-reinhardtii* and its mutants at 77-K. Photosynth Res 27: 157–168.

Martinez OE (1987) 3000 Times grating compressor with positive group-velocity dispersion: Application to fiber compensation in 1.3–1.6 μm region. IEEE J Quantum Electron QE-23: 59–64

Monshouwer R, Abrahamsson M, van Mourik F and van Grondelle R (1997) Superradiance and exciton delocalization in bacterial photosynthetic light-harvesting systems. J Phys Chem B 101: 7241–7248.

Ohtani H, Ishikawa M, Itoh H, Takiguchi Y, Urakami T and Tsuchiya Y (1990) Picosecond fluorescence spectroscopy of purple membrane in *halobacterium halobium* with a photon-counting streak camera. Chem Phys Lett 168: 493–498

Ohtani H, Kaneko M, Ishikawa M, Kamiya N and Yamamoto N (1999) Picosecond-millisecond dual-time base spectroscopy of fluorescent photointermediates formed in the purple membrane of *halobacterium halobium.* Chem Phys Lett 299: 571–575

Pal, SK, Peon J and Zewail AH (2002) Biological water at the protein surface: Dynamical solvation probed directly with femtosecond resolution. Proc Natl Acad Sci USA 99: 1763–1768

Palacios MA, de Weerd FL, Ihalainen JA, van Grondelle R, and van Amerongen H (2002) Superradiance and exciton (de)localization in light-harvesting complex II from green plants? J Phys Chem B 106: 5782–5787

Pellegrino F, Dagen A, Sekuler P and Alfano RR (1983) Temperature-dependence of the 735-nm fluorescence kinetics from

spinach measured by picosecond laser-streak camera system. Photobiochem Photobiophys 6: 15–23

Petushkov VN, van Stokkum IHM, Gobets B, van Mourik F, Lee J, van Grondelle R, and Visser AJWG (2003) Ultrafast fluorescence relaxation spectroscopy of 6,7-dimethyl-(8-ribityl)-lumazine and riboflavin, free and bound to antenna proteins from bioluminescent bacteria. J Phys Chem B 107: 10934–10939

Sauer K and Debreczeny M (1996) Fluorescence. In: Amesz J and Hoff AJ (eds) Biophysical Techniques in Photosynthesis (Advances in Photosynthesis and Respiration, Vol 3), pp 41–61. Kluwer Academic Press, Dordrecht

Schiller NH and Alfano RR (1980) Picosecond characteristics of a spectrograph measured by a streak camera/video readout system. Opt Commun 35: 451–454

Sowinska M, Heisel F, Miehe JA, Lahg M, Lichtenthaler HK and Tomasini F (1996) Remote sensing of plants by streak camera lifetime measurements of the chlorophyll *a* emission. J Plant Physiol 148: 638–644

Tars M, Ellervee A, Wasielewski MR and Freiberg A (1998) Biomolecular electron transfer under high hydrostatic pressure. Spectrochim Acta A 54: 1177–1189

Uhring W, Zint CV, Summ P, and Cunin B (2003) Very high long-term stability synchroscan streak camera. Rev Sci Instrum 74: 2646–2653

van den Berg PAW, Mulrooney SB, Gobets B, van Stokkum IHM, van Hoek A, Williams CH Jr, and Visser AJWG (2001) Exploring the conformational equilibrium of thioredoxin reductase: Characterization of two catalytically important states by ultra-fast flavin fluorescence spectroscopy. Protein Science 10: 2037–2049

van Mourik F, Frese RN, van der Zwan G, Cogdell RJ, and van Grondelle R (2003) Direct observation of solvation dynamics and dielectric relaxation in the photosynthetic light-harvesting-2 complex of *Rhodopseudomonas acidophila*. J Phys Chem B 107: 2156–2161

van Mourik F, Groot M-L, van Grondelle R, Dekker JP and van Stokkum IHM (2004) Global and target analysis of fluorescence measurements on Photosystem II reaction centers upon red excitation. Phys Chem Chem Phys 6: 4820–4824

van Stokkum IHM (2005) Global and target analysis of time resolved spectra. Lecture notes Troisième Cycle de la Physique en Suisse Romande, March 14–24, 88 pp.

van Stokkum IHM and Bal HE (2006) A problem solving environment for interactive modelling of multiway data. Concurrency Computat: Pract Exper 18: 263–269

van Stokkum IHM, Larsen DS, and van Grondelle R (2004) Global and target analysis of time resolved spectra. Biochim Biophys Acta 1657, 82–104, and 1658, 262 (Erratum)

van Stokkum IHM, Gobets B, Gensch T, van Mourik F, Hellingwerf KJ, van Grondelle R and Kennis JTM (2006) (Sub)-picosecond spectral evolution of fluorescence in photoactive proteins studied with a synchroscan streak camera system. Photochem Photobiol 82: 380–388

Vengris M, van der Horst MA, Zgrablić G, van Stokkum IHM, Haacke S, Chergui M, Hellingwerf KJ, van Grondelle R and Larsen DS (2004) Contrasting the excited-state dynamics of the photoactive yellow protein chromophore: Protein vs. solvent effects. Biophys J 87: 1848–1857

Vilchiz VH, Kloepfer JA, Germaine AC, Lenchenkov VA and Bradforth SE (2001) Map for the relaxation dynamics of hot photoelectrons injected into liquid water via anion threshold photodetachment and above threshold solvent ionization. J Phys Chem A 105: 1711–1723

Watanabe M, Koishi M, Fujiwara M, Takeshita T and Cieslik W (1994) Development of a new fluorescence decay measurement system using two-dimensional single-photon counting. J Photochem Photobiol A: Chem 80: 429–432

Wiessner A and Staerk H (1993) Optical design considerations and performance of a spectro-streak apparatus for time-resolved fluorescence spectroscopy. Rev Sci Instrum 64: 3430–3439

Yatskou MM, Koehorst RBM, van Hoek A, Donker H, Schaafsma TJ, Gobets B, van Stokkum IHM and van Grondelle R (2001) Spectroscopic properties of a self-assembled zinc porphyrin tetramer. II. Time-resolved fluorescence spectroscopy. J Phys Chem A 105: 11432–11440

Zavoiski EK and Fanchenko SD (1965) Image converter high-speed photography with 10^{-9}–10^{-14} sec time resolution. Appl Optics 4: 1155–1167